

## THE NEW MINERAL NULLAGINITE AND ADDITIONAL DATA ON THE RELATED MINERALS ROSASITE AND GLAUKOSPHERITE

E.H. NICKEL

*Division of Mineralogy, CSIRO, Private Bag, P.O., Wembley,  
Western Australia 6014, Australia*

L.G. BERRY

*Department of Geological Sciences, Queen's University,  
Kingston, Ontario K7L 3N6*

### ABSTRACT

Nullaginite,  $\text{Ni}_2(\text{OH})_2\text{CO}_3$ , is closely related to rosasite,  $(\text{Cu},\text{Zn})_2(\text{OH})_2\text{CO}_3$ , and glaukosphaerite,  $(\text{Cu},\text{Ni})_2(\text{OH})_2\text{CO}_3$ . It occurs as nodular grains and as cross-fibre veinlets in a nickel-rich assemblage from the Otway deposit, Nullagine district, Western Australia. Unit-cell parameters from X-ray fibre rotation and TED patterns and refined from powder data are  $a = 9.236(3)$ ,  $b \approx 12.001(6)$ ,  $c = 3.091(2)$  Å,  $\beta = 90.48(7)^\circ$ , possible space group  $P2_1/m$ . Strongest powder-diffraction lines are  $7.30(30b)$ , variable  $(110)$ ,  $5.04(30)(120)$ ,  $4.62(40)(200)$ ,  $3.66(40)(220,130)$ ,  $2.579(100)(201)$ ,  $2.557(90)(201)$ ,  $1.545(30)(002)$ ,  $1.541(30)(600)$ . The mineral is bright green and slightly pleochroic, with maximum absorption normal to fibre length  $c$ . Indices of refraction are  $\alpha = 1.67$ ,  $\beta \sim \gamma = 1.78$ . Extinction  $X\wedge c = 6^\circ$ . S.G. is  $3.56(3)$  (meas.) and  $4.07$  (calc.); the large discrepancy is attributed to the presence of admixed water in the specimen. Indentation hardness is  $VHN_{30} = 34(9)$ .

New X-ray-diffraction and TED data on rosasite from Bakara, Bulgaria, give refined unit-cell parameters  $a = 9.366(3)$ ,  $b = 12.116(4)$ ,  $c = 3.127(1)$  Å,  $\beta = 90.11(4)^\circ$ ; possible space group  $P2_1/m$ . X-ray crystallographic data for glaukosphaerite from Kasompi, Zaire, are consistent with two patterns having similar  $a^*$  and  $b^*$  parameters. One has an orthorhombic- $A$  lattice with  $a = 9.354(2)$ ,  $b = 23.954(4)$ ,  $c = 3.128(1)$  Å; possible space group  $Ammm$ ; the other has a monoclinic lattice with  $a = 9.35(1)$ ,  $b = 11.97(1)$ ,  $c = 3.13(1)$  Å,  $\beta = 96(1)^\circ$ , similar to that of malachite. Structural studies and additional electron-microprobe analyses are needed further to elucidate the relations between these two minerals.

**Keywords:** nullaginite, rosasite, glaukosphaerite, new mineral, Otway deposit, Nullagine district, Western Australia, Ni hydroxy carbonate, X-ray powder data.

### SOMMAIRE

La nullaginite  $\text{Ni}_2(\text{OH})_2\text{CO}_3$ , la rosasite  $(\text{Cu},\text{Zn})_2(\text{OH})_2\text{CO}_3$  et la glaukosphérite  $(\text{Cu},\text{Ni})_2(\text{OH})_2\text{CO}_3$  sont étroitement apparentées. On trouve la

nullaginite, espèce nouvelle, en nodules et en veinules à fibres transverses dans un assemblage riche en nickel découvert dans le gisement d'Otway (district de Nullagine, Australie occidentale). Ses paramètres réticulaires, déterminés sur diagrammes de fibre et de poudre, ainsi que par TED, sont:  $a$  9.236(3),  $b$  12.001(6),  $c$  3.091(2) Å,  $\beta$  90.48(7)°, groupe spatial possible  $P2_1/m$ . Les huit raies les plus intenses du cliché de poudre [ $d_{hkl}(I)(hkl)$ ] sont: 7.30(30b, variable)(110), 5.04(30)(120), 4.62(40)(200), 3.66(40)(220,130), 2.579(100)(201), 2.557(90)(201), 1.545(30)(002), 1.541(30)(600). D'un vert brillant, ce minéral est légèrement pléochroïque, avec absorption maximum perpendiculairement à l'axe de la fibre ( $\sim X\wedge c = 6^\circ$ ). Les indices de réfraction sont  $\alpha$  1.67,  $\beta \sim \gamma$  1.78. On attribue la différence entre densité mesurée [3.56(3)] et calculée [4.07] à la présence d'eau dans le spécimen. La dureté par indentation,  $VHN_{20}$ , est de 34(9).

Pour la rosasite de Bakara (Bulgarie), les données nouvelles de diffraction X et de TED ont permis l'affinement des paramètres du réseau:  $a$  9.366(3),  $b$  12.116(4),  $c$  3.127(1) Å,  $\beta$  90.11(4)°, groupe spatial possible  $P2_1/m$ . Les résultats de diffraction X obtenus sur la glaukosphérite de Kasompi (Zaire) donnent des paramètres  $a^*$  et  $b^*$  semblables pour tous les spécimens et conduisent à l'un ou l'autre de deux réseaux: 1) orthorhombique- $A$ ,  $a$  9.354(2),  $b$  23.954(4),  $c$  3.128(1) Å, groupe spatial possible  $Ammm$ , 2) monoclinique,  $a$  9.35(1),  $b$  11.97(1),  $c$  3.13(1) Å,  $\beta$  96(1)°, semblable à celui de la malachite. Il faudra déterminer la structure cristalline et faire plus d'analyses à la microsonde électronique pour préciser les relations entre ces deux espèces.

(Traduit par la Rédaction)

**Mots-clés:** nullaginite, rosasite, glaukosphérite, espèce nouvelle, gisement Otway, district Nullagine, Australie occidentale, hydroxy-carbonate de Ni, cliché de poudre.

### DESCRIPTION OF NULLAGINITE

#### Introduction

In the Nullagine district of Western Australia,

a nickel-rich mineral assemblage occurs in shears in serpentized peridotite, at a locality known as the Otway deposit. The principal nickel minerals, millerite, polydymite and pecoraite, occur chiefly as nodular grains. Other nickel minerals, occurring in lesser amounts, are gaspéite, otwayite, parkerite, shandite, breithauptite and nullaginite, the new mineral described in this paper. The occurrence of nullaginite was reported briefly in a general paper on the geology and mineralogy of the deposit (Nickel *et al.* 1979). Previous papers on the mineralogy of the Otway deposit describe gaspéite and pecoraite (Nickel 1973) and the recently discovered mineral otwayite,  $\text{Ni}_2(\text{OH})_2\text{CO}_3 \cdot \text{H}_2\text{O}$  (Nickel *et al.* 1977).

Nullaginite is named for the district in which it was found. Both mineral and name have been approved by the I.M.A. Commission on New Minerals and Mineral Names.

#### Occurrence

Nullaginite occurs as nodules and as veinlets. The nodules, ovoid to irregular in shape, bright green in color, up to 2 mm in diameter, are found in a matrix of chlorite and nickeloan serpentine (Figs. 1, 2). The nodules commonly contain magnetite, which is usually distributed

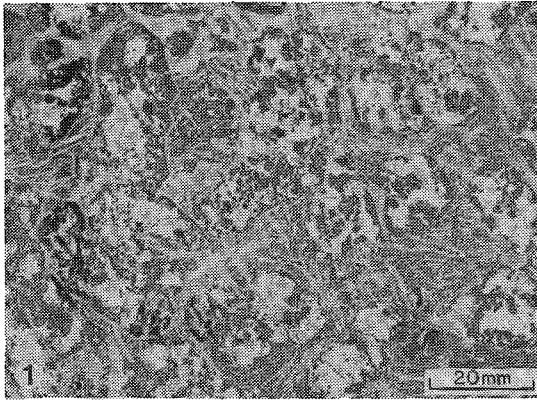


FIG. 1. Photograph of coarsely ground surface of hand specimen, sample 10025, showing altered nullaginite nodules (white), rimmed by magnetite (black), in a matrix of chlorite and nickeloan serpentine (foliated).

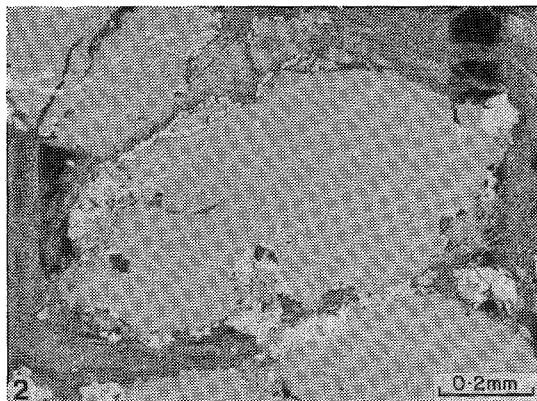


FIG. 2. Electron-backscatter micrograph of a nullaginite nodule in a polished section of sample 10025. The white mineral is magnetite.

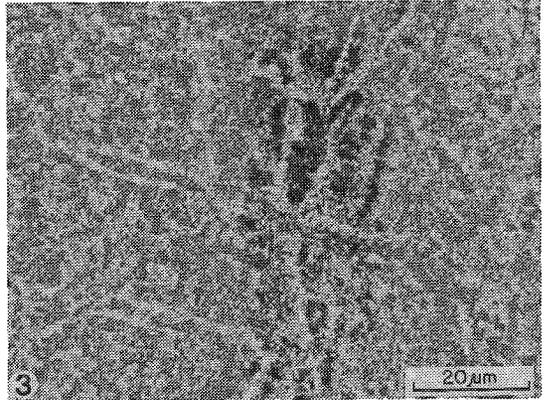


FIG. 3. Electron-backscatter micrograph of the same nodule shown in Figure 2, but at a higher magnification, showing the felted nature of the nullaginite comprising the nodule.



FIG. 4. Electron-backscatter micrograph of a polished section of sample 11052, showing zonal intensity variations in a veinlet of cross-fibre nullaginite. The white mineral on both sides of the nullaginite is pecoraite, and the dark zones in the vein are magnesian pecoraite. The line scan shown in Figure 5 was made along the line A-B.

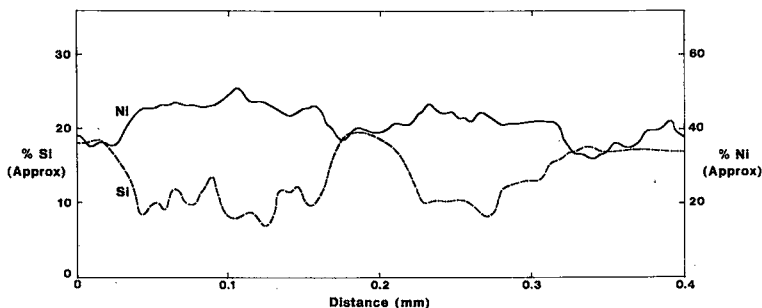


FIG. 5. Electron-microprobe line scan across the veinlet shown in Figure 4.

around the grain margins. At high magnifications under the scanning electron-microscope (SEM), the nodules are seen to consist of a felted intergrowth of crystallites (Fig. 3). The nodular nullaginite is commonly intergrown with pecoraite, which forms nodules virtually identical in appearance to those of nullaginite. In a few samples the nullaginite has been altered to a pale green, chalky material (Fig. 1) that gives X-ray-diffraction patterns corresponding to nullaginite and gaspéite. These chalky nodules seem to be a product of decomposition of the nullaginite.

The nullaginite occurring in veinlets consists of tiny cross-fibre crystallites and is virtually identical in appearance to otwayite (Nickel *et al.* 1977). The nullaginite is generally intergrown with pecoraite, locally in a strikingly zoned fashion; this is particularly evident in SEM electron-backscatter images (Fig. 4). In such images, the intensity of backscattered radiation is a function of the average electron-backscatter coefficient, which is, in turn, a direct function of composition. The vein nullaginite shown in Figure 4 can be seen to exhibit compositional differences normal to the veinlet walls. Comparison with the electron-microprobe line scan across the veinlet (Fig. 5) indicates that the differences are attributable, in part, to variations in silica content. The high silica content along the margins of the vein is due to pecoraite, which gives a relatively high electron-backscatter intensity. However, the high content of silica within the nullaginite veinlet itself corresponds to a relatively low intensity due, at least in part, to the presence of magnesium; this suggests that the low-intensity phase that forms the core of the veinlet in Figure 4 is probably magnesian pecoraite.

#### Crystallography

Three small needle-like fragments (approx-

mately 0.5 x 0.05 mm) were examined by rotation and Weissenberg X-ray-diffraction methods. One fragment yielded a powder diagram on rotation, and two gave fibre diagrams with a clear separation of zero and first levels (a separation of  $\sim 20$  mm with  $\text{Co } K\alpha$  radiation in a camera of radius  $360/2\pi$  mm), indicating a period of  $c = 3.1(1)$  Å, with all diffractions extended 2 to 5 mm along the powder arcs to either side of the median layer-line position. No reflections show spot maxima as observed on similar films of glaukosphaerite. On the zero-level Weissenberg film,  $hk0$  reflections extend almost the full length (100 mm) of the exposed film, parallel to the rotation axis. The reflections recorded on the zero-layer line of the rotation films and on the zero-layer Weissenberg film are, for the most part, very sharp arcs or lines; the reflections can be indexed on orthogonal axes with  $a = 9.23$ ,  $b = 11.95$  Å (average from several films), corresponding to  $a$  and  $b$  of malachite and glaukosphaerite (Table 1); a few weak and diffuse reflections are nearly complete powder rings. The most intense diffractions on the rotation films are a set of four arcs with maxima on the first layer line; these arcs are much broader (*ca.* 0.3 mm) than the zero-level diffractions and do not extend to the zero-level row. A rotation film-chart overlay gives an average value for these diffractions of  $\theta = 20.5^\circ$ ,  $d = 2.56$  Å, which corresponds closely to the average of  $d_{201}$  and  $d_{201}$  derived from transmission electron-diffraction (TED) and powder-pattern indexing.

Transmission electron-diffraction patterns from six random fragments of nullaginite give  $a = 9.27(8)$ ,  $c = 3.13(4)$  Å,  $\beta = 90.4(3)^\circ$ . The patterns were recorded on plates after trial-and-error tilting of the grain about any horizontal axis in the plane of the stage to improve the pattern. The patterns display twofold rotational symmetry, with interaxial angles between  $90.1$  and  $91.4^\circ$ .

TABLE 1. MALACHITE, ROSASITE AND RELATED MINERALS

Name	Formula	Sp. Gr.	aÅ	bÅ	cÅ	$\alpha$	$\beta$	$\gamma$	Reference
malachite	$\text{Cu}_2(\text{OH})_2\text{CO}_3$	$P2_1/a$ or $P2_1$	9.49 9.502	12.00 11.974	3.24 3.24	-	98°42' 98°45'	-	Ramsdell & Wolfe (1950) Swanson <i>et al.</i> (1960)
rosasite	$(\text{Cu}, \text{Zn})_2(\text{OH})_2\text{CO}_3$	$P2_1/m$ or $P2_1$	9.366	12.116	3.127	-	90°06'	-	(synthetic) This study: Bakara, Bulgaria
zincrosasite	$(\text{Zn}, \text{Cu})_2(\text{OH})_2\text{CO}_3$	-	-	-	-	-	-	-	Strunz (1959)
glaukosphaerite	$(\text{Cu}, \text{Ni})_2(\text{OH})_2\text{CO}_3$	-	9.34	11.93	3.07	-	90-91°	-	Pryce & Just (1974)
glaukosphaerite	-	-	9.364	11.93	3.413	-	92.25°	-	Jambor (1976a) Kambalda, W.A.
glaukosphaerite	-	-	9.368	11.99	3.387	-	92.12°	-	" Kasompi, Zaire
glaukosphaerite	-	-	9.52	12.05	3.218	95.45°	92.92°	90.78°	Deliens & Piret (1980) Kasompi, Zaire
glaukosphaerite	-	$Ammm$ $P2_1/a$	9.354 9.35	23.954 11.97	3.128 3.13	-	-	-	This study Kasompi, Zaire
glaukosphaerite	-	$Ammm$	9.363	23.896	3.138	-	-	-	This study Kambalda, W.A.
kolwézite	$(\text{Cu}, \text{Co})_2(\text{OH})_2\text{CO}_3$	-	9.50	12.15	3.189	93.32°	90.74°	91.47°	Deliens & Piret (1980) Kolwézi, Shaba
nullaginite	$\text{Ni}_2(\text{OH})_2\text{CO}_3$	$P2_1/m$ or $P2_1$	9.236	12.001	3.091	-	90°48"	-	This study, Otway deposit Nullagine, W.A.
Intermediate compound in topo- tactic thermal decomposition of artinite	$\text{Mg}_2(\text{OH})_2\text{CO}_3$	-	9.34	3.15	12.18	-	90°	-	Günter & Oswald (1977)
mcguinnessite	$(\text{Mg}, \text{Cu})_2(\text{OH})_2\text{CO}_3$	-	9.34	12.18	3.15	-	-	90°	" (rosasite setting)
									name approved, no data published, Oswald & Crook (1979)

From one other single grain, five patterns obtained at angles of tilt of 3° N, S, E and W and from the original position about NS and EW axes of the stage give  $a = 9.20(6)$ ,  $c = 3.09(3)$  Å,  $\beta = 90.9(1)^\circ$ . In this set of patterns, the most intense pair of diffractions is consistently  $201$  and  $20\bar{1}$ , lying in the obtuse angle between  $a^*$  and  $c^*$ . The microscope was operated under the same settings throughout; the patterns were externally calibrated with graphite. No effort was made to tilt grains oriented on  $h0l$  to other zero levels because it is difficult to rotate a grain about a particular axis, and the normally short life of a grain in the beam precludes extensive reorienting.

The X-ray powder-diffraction pattern of nullaginite is very similar to those of rosasite and glaukosphaerite (Table 2). A notable feature of the pattern obtained from a high-resolution Guinier camera, although not observable on a normal Debye-Scherrer pattern, is the splitting of the  $201-20\bar{1}$  doublet. The intensity of the 7.3 Å line varies from pattern to pattern and appears to be due, at least in part, to different amounts of an admixed serpentine mineral, probably pecoraite.

The similarity of the zero-level diffractions in rotation and Weissenberg films of malachite, glaukosphaerite and nullaginite determines the indexing of many of the high  $d$ -value powder lines; these lines are sharp and not split into doublets. The first-level Weissenberg film estab-

lishes the correct indexing of non- $hk0$  reflections in malachite and glaukosphaerite. In nullaginite the distinctive doublet at  $d = 2.579$  and  $d = 2.557$  provides a strong clue to the indexing. TED diagrams ( $h0l$ ) have  $201$  with  $d = 2.58$  and  $20\bar{1}$  with  $d = 2.55$  as the strongest diffractions, with  $I_{201} > I_{20\bar{1}}$ . This indexing is supported by a strong first-layer diffraction on the fibre-rotation diagram ( $201$  and  $20\bar{1}$  unresolved). Refinement of the powder data of nullaginite yields  $a = 9.236(3)$ ,  $b = 12.001(6)$ ,  $c = 3.091(2)$  Å,  $\beta = 90.48(7)^\circ$ ; 1 line of  $l = 10$  and three of  $l = 5$ , of uncertain  $hkl$ , are presumed due to unidentified impurities. The refinement identifies a broad line with  $d = 2.932$  as  $101$  and  $10\bar{1}$ , establishing the possible space-group as  $P2_1/m$  or  $P2_1$ .

### Composition

Attempts were made to concentrate sufficient amounts of pure material for chemical analysis, both by hand-picking and heavy-liquid and magnetic separation procedures; all concentrates were found to contain substantial amounts of impurities, especially pecoraite and gaspéite. Eventually these attempts were abandoned in favor of the electron microprobe. This is not entirely satisfactory, since hydroxyl, carbonate and possibly water must be inferred by calculation; nevertheless, there was no reasonable alternative.

TABLE 2. X-RAY POWDER-DIFFRACTION PATTERNS OF NULLAGINITE, ROSASITE AND GLAUKOSPHAERITE

NULLAGINITE							ROSASITE				GLAUKOSPHAERITE						
Otway, Nullagine, West Australia							Bakara, Bulgaria				Kasompi, Zaire					Kambalda, W.A.	
a=9.236, b=12.001, c=3.091Å, β=90°29'							a=9.366, b=12.116, c=3.127Å, β=90°06'				a=9.4, b=24.0, c=3.1Å						
I	d <sub>meas</sub>	hkl	d <sub>calc.</sub>	I <sub>r</sub>	d <sub>r+w</sub>	I <sub>w</sub>	I	d <sub>meas</sub>	hkl	d <sub>calc.</sub>	I	d <sub>meas</sub>	hkl	d <sub>calc.</sub>	I <sub>w</sub>	I	d <sub>meas</sub>
30b	7.302	110	7.319	w	7.40	w	10	7.46	110	7.410	10	7.398	120	7.372	w	20	7.413
<5b	6.018	020	6.001	w	6.01	w	60	6.06	020	6.058	50	6.002	040	5.988	s	40	5.991
30	5.038	120	5.032	m	5.04	vs	80	5.094	120	5.087	55	5.048	140	5.043	s	50	5.048
40	4.619	200	4.618	w	4.61	m	15	4.696	200	4.683	10	4.686	200	4.677	w	20	4.693
40	3.660	{130 220}	{3.671 3.660}	s	3.67	s	100	3.708	{130 220}	{3.708 3.705}	100	3.689	240	3.686	vs	80	3.690
													160	3.672	w	20	3.665
20	3.097	001	3.091				40	3.025	310	3.029	10	3.037	260	3.036		—	—
10	3.001	040	3.001	w	3.03		40b	2.967	{101 140 111}	{2.968 2.882 2.880}	20	3.018	320	3.017	m	30	3.021
10	2.981	310	2.982	w	2.98	m	20	2.880	{111 121}	{2.880 2.665}	20	2.994	080	2.994	m	20	2.988
20b	2.932	{101 101}	{2.939 2.924}				20	2.774	320	2.775	40b	2.940	111	2.944	s	70	2.952
5*	2.878	ni	—				5	2.691	{201 201}	{2.665 2.603}	15	2.852	180	2.852	w	20	2.850
							70b	2.601	{201 201}	{2.599 2.599}	10	2.766	340	2.755	m	30	2.769
20	2.854	{111 140}	{2.855 2.854}	w	2.84	w	70	2.542	240	2.543	80vb	2.586	211	2.585	vs	100b	2.591
20	2.740	320	2.739	vw	2.73		15b	2.507	ni	—	60	2.523	280	2.522	vs	50	2.517
10	2.726	ni	—				15	2.471	330	2.470	30b	2.484	231	2.472	s	70b	2.484
10b	2.653	121	2.642				vf	2.360	150?	2.346	30b	2.484	231	2.472	s	70b	2.484
100	2.579	201	2.579				50	2.342	400	2.341	30	2.459	360	2.457	m	30	2.457
90	2.557	201	2.558				<5	2.212	301	2.211	30b	2.340	400	2.339	s	35	2.343
20	2.516	240	2.516	s	2.51	s	10	2.185	420	2.184	30b	2.320	1.10.0	2.320	m	35b	2.315
10b	2.449	031	2.446				<5	2.168	311	2.172	5b	2.299	420	2.295		20	2.298
10b	2.192	301	2.191				50	2.151	250	2.152	—	—	311	2.199	m	30	2.203
							15	2.022	{430 060}	{2.026 2.019}	20	2.178	440	2.178	w	40	2.181
											35	2.131	{2.10.0 331}	{2.132 2.128}	{m m}	30b	2.132
											5b	2.017	460	2.018		25	2.018
10b	2.129	250	2.130	s	2.13	s	5b	1.982	ni	—	—	—	351	2.005	w	25	2.001
5	2.117	141?	2.099				15	1.973	{241 160}	{1.974 1.974}	20	1.996	0.12.0	1.996	m	20	1.989
5b	2.095	141	2.094				15	1.912	350	1.914	15	1.951	1.12.0	1.952	w	20	1.947
5b	2.000	{060 430}	{2.000 2.000}	m	2.00	w	5	1.877	151	1.877	20	1.900	3.10.0	1.900	w	30	1.896
5	1.835	{260 440}	{1.835 1.830}	w	1.83	w	20	1.855	260	1.854	—	—	500	1.871		10	1.873
10	1.763	{520 421}	{1.765 1.761}	m	1.76	w	20	1.788	520	1.790	5b	1.846	520	1.848		30	1.851
5b	1.736	251?	1.750				15b	1.746	ni	—	20	1.785	540	1.786	w	35	1.787
30	1.545	002	1.545				20	1.699	{530 431}	{1.699 1.699}	20b	1.740	451	1.744	m	50	1.743
30	1.541	600	1.539				15	1.663	161	1.669	5b	1.694	560	1.694	w	20	1.694
20b	1.528	{521 610}	{1.527 1.527}				5	1.595	{441 261}	{1.595 1.594}	5b	1.682	{1.14.0 3.12.0}	{1.683 1.681}	{w w}	20	1.678
5b	1.368	{640 312}	{1.370 1.367}	m	1.367		10	1.570	002	1.564	5b	1.646	471	1.643	m	40b	1.649
							5	1.541	{102 102}	{1.543 1.542}	20b	1.576	531	1.574	w	25b	1.577
							10	1.512	620	1.512	15b	1.527	122	1.530		50	1.556
							5	1.494	{531 122}	{1.494 1.494}	5b	1.508	640	1.509	w	50b	1.531
							10	1.481	{550 451}	{1.482 1.482}	5b	1.497	0.16.0	1.497	vw	15	1.510
							5	1.440	{132 222}	{1.440 1.440}	20b	1.474	5.10.0	1.474	w	35	1.476
							10	1.412	541	1.419	5b	1.398	302	1.398		30b	1.397
							10	1.387	{640 611}	{1.388 1.386}	10b	1.383	680	1.383	w	30	1.382

I<sub>r</sub> = Intensities estimated from rotation patterns; I<sub>w</sub> = Intensities estimated from Weissenberg patterns; I, d<sub>meas</sub> from Guinier films, Cu/Ni, ThO<sub>2</sub> internal standard; d<sub>r+w</sub> measured from rotation and 0-level Weissenberg films; ni = not indexed.

TABLE 3. ELECTRON-MICROPROBE ANALYSIS OF NODULAR NULLAGINITE, SAMPLE 10025

	Wt%	Recalc. to 100% A	100% B	Atomic Props.	Ni <sub>2</sub> (OH) <sub>2</sub> CO <sub>3</sub> (wt%)
Ni	49.4	46.76	53.96	1.93	55.53
Mg	0.56	0.51	0.59	0.05	
Cr	0.23	0.25	0.29	0.01	
Fe	0.15	0.15	0.17	<0.01	
Cu	0.07	0.08	0.09	<0.10	
Si	1.88	-	-	-	
OH (calc.)	14.44	14.07	16.24	2.00	16.09
CO <sub>3</sub> (calc.)	22.70	24.84	28.66	1.00	28.38
H <sub>2</sub> O (?)	-	13.34	-	-	
	89.43	100.00	100.00		

Both A and B are corrected for 8.6% pecoraite. A assumes that the shortfall from 100% is due to H<sub>2</sub>O; in B no excess is assumed, and the analysis is recalculated to 100%. The atomic proportions are taken from the B recalculation.

Both nodular and veinlet varieties of nullaginite were analyzed in five different samples. The results of all analyses are similar, showing appreciable but variable amounts of silicon. The results of one analysis (of the nullaginite nodule shown in Fig. 2) are given in Table 3. The analytical results are an average obtained from five different spots on the same nodule.

The Si is assumed to be due to an impurity; as X-ray-diffraction patterns show a line of variable intensity at 7.3 Å, one of the strongest lines in the X-ray-diffraction pattern of serpentine, it is concluded that the observed Si is due to the presence of a serpentine mineral. Electron-microprobe line-scans across the serpentine mineral associated with nullaginite show that it generally has a high Ni content (Fig. 5); for the purpose of the calculations, it was therefore assumed that the serpentine mineral responsible for the Si is pecoraite, with a composition corresponding to that reported by Nickel (1973). On this assumption, the 1.88% Si shown in Table 2 represents 8.6% pecoraite.

After the pecoraite correction was made, there was still a shortfall of 10.61%. In one recalculation (A, Table 3), this shortfall was attributed to admixed water; as is demonstrated below, optical and physical properties tend to support this assumption. Analysis B assumes the mineral to be anhydrous, by analogy with rosasite and glaukosphaerite. The atomic proportions are calculated on a cation sum of 2; the proportions of OH and CO<sub>3</sub> slightly exceed 2 and 1, respectively, because of the trivalent charge of Cr.

An electron-microprobe line-scan across the veinlet illustrated in Figure 4 is reproduced in Figure 5. This shows that appreciable Si occurs in even the purest part of the nullaginite veinlet. A high-resolution electron-backscatter image of the analyzed nodule (Fig. 3) shows variations

in intensity presumably attributable to differences in atomic number. These variations were too subtle to be picked up by microprobe line-scans; their interpretation therefore remains unclear. Perhaps they represent minor variations in the amount of water held by the nullaginite.

Infrared absorption analyses were undertaken in an attempt to obtain independent confirmation for assumptions made on the anions present in nullaginite. Absorption peaks corresponding to H<sub>2</sub>O, OH and CO<sub>3</sub> were recorded, but because of impurities of pecoraite and gaspéite in the sample, the data did not provide significant additional information.

#### Optical and physical properties

Nullaginite is bright green. In its nodular form it has a dull, clay-like lustre; in cross-fibre veinlets it has a silky sheen. In transmitted light it is pale green and weakly pleochroic, with absorption slightly greater normal to the fibre axis (*c*) than parallel to it. Indices of refraction are  $\alpha = 1.67$ ,  $\beta \sim \gamma = 1.78$ . Extinction  $X\lambda c = 6^\circ$ . Because of the extremely fine size of crystallites, it was not possible to measure the optic angle or to uniquely determine the optical orientation. However, as *X* is close to *c*, the *b* crystallographic axis should correspond to *Y* or *Z*.

The indices of refraction are appreciably lower than those reported for glaukosphaerite (Pryce & Just 1974, Deliens 1975), which is contrary to expectations, since NiO has a higher specific refractivity than CuO (Mandarino 1976). This tends to confirm that nullaginite contains some admixed water or other submicroscopic intergrown impurity.

The specific gravity of tiny particles was measured by suspension in Clerici solution. Values obtained ranged between 3.528 and 3.606, with an average of 3.56. The calculated specific gravity, using a unit-cell volume of 342.6 Å<sup>3</sup> and the recalculated composition (B, Table 3), and assuming *Z* = 4, is 4.07. However, if the specific gravity is corrected for the 13.34% water suggested by recalculation A, then a value of 3.660 is obtained, which is in reasonable agreement with the measured value. If the excess water were incorporated into the structural formula, the calculated specific gravity would increase, widening the discrepancy between measured and calculated values.

A Gladstone-Dale calculation (Mandarino 1976) of the mean index of refraction, using the measured specific gravity and the empirical

composition corrected for the pecoraite impurity (recalculation A, Table 3), gives  $\bar{n} = 1.768$ . This agrees reasonably well with the mean of the measured indices of refraction:  $[2(1.78) + 1.67]/3 = 1.74$ .

The hardness of nullaginite was measured with a Vickers indenter using a 20 g load. The average of five determinations gave *VHN* 34.4(9).

#### Discussion

The close similarity of the X-ray-diffraction powder pattern of nullaginite, rosasite, zincrosasite and glaukosphaerite indicates that they are all members of the same mineral group, which should be termed the rosasite group, after the first mineral that was described (Table 1). According to present usage, the formula of the group can be expressed as  $M_2(\text{OH})_2\text{CO}_3$ , with *M* comprising Cu and Zn,  $\text{Cu} > \text{Zn}$  in rosasite,  $\text{Zn} > \text{Cu}$  in zincrosasite, Cu and Ni in glaukosphaerite and Ni alone in nullaginite. The crystal structures of minerals of the group have not been worked out, but a structure has been deduced (Günter & Oswald 1977) for  $\text{Mg}_2(\text{OH})_2\text{CO}_3$ , the decomposition product of artinite, which has a unit cell similar in dimensions, but which differs in the orientation of symmetry elements and in the systematic extinctions from those of the rosasite group of minerals. [Note that Oswald & Crook (1979) introduced the name "mcguinnessite" (without data) for  $(\text{Mg}, \text{Cu})_2(\text{OH})_2\text{CO}_3$ . The mineral and name had received prior I.M.A. approval\*.] According to Günter & Oswald (1977), the structure consists of  ${}^{\text{VI}}\text{Mg}^{\text{III}}(\text{OH})_3^{\text{II}}(\text{CO}_3)$  sheets of edge-sharing octahedra parallel to 102, corresponding to 120 in malachite and rosasite; adjacent layers are connected by bridging carbonate groups. The structure allows only one kind of octahedral composition, whereas the malachite structure, with its two different octahedral sites, is incompatible with the topotactic relation of  $\text{Mg}_2(\text{OH})_2\text{CO}_3$  with artinite. If this structure proves to be the correct one for the rosasite group of minerals, there would appear to be little justification to regard glaukosphaerite as a separate species. If the Cu end-member is called rosasite, and the Ni end-member, nullaginite, then the mineral originally described as rosasite,  $(\text{Cu}, \text{Zn})_2(\text{OH})_2\text{CO}_3$ , would be more correctly termed zincian rosasite. Glaukosphaerite,  $(\text{Cu}, \text{Ni})_2(\text{OH})_2\text{CO}_3$ , is simply a nickeloan rosasite.

All evidence on nullaginite indicates that the mineral contains nonstructural water not represented in the formula  $\text{Ni}_2(\text{OH})_2\text{CO}_3$ ; the question arises whether the formula should, perhaps, be given as  $\text{Ni}_2(\text{OH})_2\text{CO}_3 \cdot n\text{H}_2\text{O}$ . A crystal-structure determination is needed to give the answer.

Regarding the origin of the nullaginite, in its veinlet form it is late in the paragenesis and may even be a supergene product (Nickel *et al.* 1979). It is more difficult to determine the origin of the nodular variety, but the weight of evidence regarding the other nodular minerals in the deposit suggests that they were formed as the result of hydrothermal activity; they may have been precipitated from a gel medium (Nickel *et al.* 1979). Crystallization in a gel would explain the intergrown silica and the water that is assumed to be in excess of the formula requirements.

#### NEW X-RAY DATA ON ROSASITE AND GLAUKOSPHERITE (LGB)

##### Rosasite

New Guinier powder data for rosasite from Bakara, Bulgaria, are presented in Table 1 for comparison with nullaginite and glaukosphaerite. TED diagrams from two grains are similar to those of nullaginite and are indexable as *h0l* with  $a = 9.3$ ,  $c = 3.15 \text{ \AA}$ ,  $\beta = 90^\circ 55'$ ;  $\bar{1}01$ ,  $\bar{2}01$  and  $\bar{3}01$  appear consistently as the strongest diffractions. Mirror symmetry is distinctly lacking, although TED intensities are unreliable. This information leads to refinement of the powder data with cell dimensions  $a = 9.366(3)$ ,  $b = 12.116(4)$ ,  $c = 3.127(1) \text{ \AA}$ ,  $\beta = 90.11(4)^\circ$ ; a few weak diffractions with uncertain indices are presumably due to impurities. The refinement identifies a broad line at  $d = 2.967$  as  $\bar{1}01$  and  $101$ , confirming the possible space-groups as  $P2_1/m$  or  $P2_1$ . Rosasite specimens from Bakara (Bulgaria), Durango (Mexico) and Rosas (Sardinia) give virtually identical powder-diffraction patterns.

New electron-microprobe analyses of rosasite from Bakara, given in Table 4, are compared with unpublished analyses obtained by Jiri Just (pers. comm.) at CSIRO in 1973 on specimens from Durango, Mexico (#1789 CSIRO) and from Rosas, Sardinia (British Museum, Natural History, 1924 167). There is no distinctive trend in the ratio of Zn to total metal from the centre of a rosette to the border.

##### Glaukosphaerite

Previous work: Glaukosphaerite,  $(\text{Cu}, \text{Ni})_2$

\*Note added in proof: a full description of mcguinnessite has been published by Erd *et al.* (1981).

TABLE 4. ROSASITE, PARTIAL ANALYSES

Bakara, Bulgaria						
	wt. % electron microprobe				outer	chem. anal. <sup>1</sup>
	inner					
Cu	33.2	32.6	33.6	30.6	31.1	37.50
Zn	24.5	25.8	23.6	26.6	25.2	31.09
Ni	0.28	0.24	0.20	0.21	0.22	nd
Co	0.02	0.00	0.00	0.00	0.00	nd
Fe	0.01	0.00	0.01	0.00	0.00	nd
Zn metals	0.42	0.43	0.40	0.46	0.44	0.45

Durango, Mexico, J. Just (unpublished)						
	wt. % 13 analyses <sup>2</sup>			wt. % 7 analyses		
	range		mean	range		mean
Cu	32.2	to 35.1	33.7	30.3	to 32.9	31.6
Zn	20.8	to 22.3	21.6	20.1	to 24.3	22.2
Zn metals			0.39			0.40

Rosas, Sardinia, J. Just (unpublished)			
	wt. % 13 analyses <sup>2</sup>		
	range		mean
Cu	40.0	to 43.0	41.5
Zn	11.1	to 14.4	12.7
Zn metals			0.24

<sup>1</sup>Mincheva-Stefanova (1961)    <sup>2</sup>no apparent trend in ratio from centre to rim of rosette

(OH)<sub>2</sub>CO<sub>3</sub>, with Cu/Ni = 1.4–1.5, was first described by Pryce & Just (1974) from specimens found at several localities in Western Australia from 1967 to 1973. The Australian material did not yield complete single-crystal X-ray data but the powder pattern, with the exception of three lines, could be indexed on a cell similar to that of malachite, except for a  $\beta$  angle close to 90°.

A similar mineral, (Cu,Ni)<sub>2</sub>(OH)<sub>2</sub>CO<sub>3</sub>, with Cu/Ni = 1.73 from Kasompi (southern Shaba, Zaire) was described by Deliens (1975). The powder data for the minerals from Kambalda (W.A.) and from Kasompi are very similar. Jambor (1976a) suggested a variation on the indexing that still left one line ( $d = 2.928$ ) unindexed, resulting in a cell closer to that of malachite.

The opportunity to re-examine this problem arose during a sabbatical-leave visit by the author to CSIRO (Perth, W.A.) in 1976. Additional Australian specimens had become available, and a specimen of the Kasompi material had kindly been supplied by Michel Deliens at the request of Jiri Just. Gandolfi patterns on a 57.3 mm powder camera with Co/Fe radiation, and Guinier focusing-camera films (Cu/Ni) with ThO<sub>2</sub> as an internal standard, confirm the previously published powder data, including the

doublet at  $d = 2.95$  and  $2.93$ . This doublet is not resolved in the films of the Kasompi material and appears as a single broad line.

*Weissenberg study:* Initially, a thin prismatic crystal of glaukosphaerite from Kasompi was mounted for Weissenberg study by M.W. Pryce of Government Chemical Laboratories at Perth. On a rotation film (Co  $K\alpha$  57.3 mm diameter) about the needle axis, the zero-layer line shows sharp reflections with streaking along powder arcs for 2 to 4 mm on either side of the layer line. The first-layer line, about 20 mm from the zero line, shows, within powder arcs, spot maxima that are more diffuse than zero-layer diffractions; not one of the powder arcs is continuous between the zero- and first-layer lines. On a zero-level Weissenberg pattern, the reflections are sharp and perpendicular to the axis, but drawn out 2–4 mm parallel to the axis, with weaker powder-diffractions connecting the stronger  $hk0$  diffractions for the full length of the film. The zero-layer pattern is almost identical to the  $hk0$ -level pattern of malachite. The first-level Weissenberg film displays a full pattern of  $hk1$  diffractions, all as distinct spots but more diffuse than those of the zero level. A reciprocal-lattice plot of the first-level Weissenberg film displays two patterns with similar  $a^*$  and  $b^*$  parameters. The stronger, more complete pattern displays  $mm2$  symmetry, but with  $b^*$  halved,  $k$  odd in  $hk1$  and even in  $hk0$ ;  $h01$  reflections are absent. This leads to an orthorhombic  $-A$  lattice with  $a = 9.5$ ,  $b = 24.0$ ,  $c = 3.1$  Å. The second, weaker pattern, displaying  $m$  symmetry, offset along  $h01$ , is readily indexable as two patterns in twin relationship, with (100) as a twin plane. This pattern is consistent with a coexisting second crystal, having a monoclinic lattice with  $a = 9.35$ ,  $b = 11.97$ ,  $c = 3.13$  Å,  $\beta = 96^\circ 0'$ , *i.e.*, similar to that of malachite. The distinctive observed reflections, all in the first level, are  $\bar{2}01$  s,  $\bar{2}11$  w,  $201$  w,  $211$  vw,  $111$  w,  $021$  vw and  $031$  vw;  $\bar{2}01$ , with  $d = 2.851$ , would coincide with  $d = 2.852$  in the powder-diffraction pattern of glaukosphaerite. No other reflections appear to be sufficiently intense to appear in the powder pattern.

A second crystal confirmed the results obtained from the first crystal and enabled the accurate location of  $a^*$  and  $b^*$  relative to the dial axis of the instrument. On a precession camera, zero- and first-level films about  $a$  and zero-level films about  $b$ , although weak, confirmed the Weissenberg indexing, especially the extinction conditions  $hkl$ , present only with  $k + l = 2n$  and characteristic of the  $A$  lattice. These

observations clearly indicate the presence of a parallel intergrowth of two phases in the Kasompi material.

**Electron diffraction:** Transmission electron-diffraction plates of glaukosphaerite give the following average cell-dimensions from  $h0l$  patterns: Kambalda, W.A.:  $a = 9.39$ ,  $c = 3.08$  Å, " $\beta$ " =  $90^\circ 30'$  (8 samples); Kasompi, Zaire:  $a = 9.42$ ,  $c = 3.12$  Å, " $\beta$ " =  $90^\circ 57'$  (10 samples). These patterns are not all of equal quality; because of poor orientation, some patterns are less complete than others. Some of the above patterns show distinct  $2mm$  symmetry and " $\beta$ " angles very close to  $90^\circ$  (within  $15'$ ). The "average  $\beta$ " is the average divergence from  $90^\circ$ , since there is no distinction between  $h0l$  and  $\bar{h}0l$  in an  $h0l$  pattern with  $2mm$  symmetry.

TED diagrams of two crystal fragments from Kambalda and three from Kasompi are zero-level patterns, ( $\bar{3}12$ ) with diffractions 260, 111,  $\bar{1}51$ , 371,  $\bar{3}\bar{1}\bar{1}.1$ , 052, 222 and  $\bar{2}\bar{1}\bar{0}.2$ . These diffractions are compatible with the  $A$ -lattice extinction condition, but not all are present on X-ray-diffraction films. An average of the measurements from these patterns gave  $a = 9.3$ ,  $b = 24.2$ ,  $c = 3.2$  Å. The orthorhombic  $A$  lattice, indicated unambiguously by  $hk0$  and  $hk1$  Weissenberg diffractions and confirmed by indexing of the zero-level ( $\bar{3}12$ ), is not confirmed by  $h0l$  diffractograms, since the systematic extinction of  $h0l$  is not observed. In TED diffractograms,  $h0l$  may well have  $h1l$  superimposed on it, especially in this case where  $d^*$  [010] is very short ( $b \sim 24$  Å and  $b^* = 1.33$  mm, on the scale of the TED diffractograms obtained here).

**Discussion:** Single-crystal Weissenberg films of the first layer  $hk1$  of the reciprocal lattice of glaukosphaerite from Kasompi, Zaire, clearly indicate that two phases are present, one orthorhombic  $A$  and the other monoclinic (twinned on 100). This relation is not evidenced in zero-layer films, TED plates or powder-diffraction patterns. One powder line with  $d = 2.852$  corresponds to  $\bar{2}01$  of the monoclinic phase (calculated 2.851), but it also corresponds to 180 in the orthorhombic  $-A$  phase. The powder-diffraction patterns of Kasompi and Kambalda glaukosphaerite are quite similar. The latter shows better resolution, especially at  $d = 2.940$  (111) in Kasompi, 2.952 (111), 2.931 (031) in Kambalda; three other weak lines fail to appear in the Kasompi pattern. The cell dimensions of the monoclinic phase, not refined from powder spacings, indicate a similarity to malachite, possibly a nickeloan variety; microprobe

analyses might confirm this. The higher nickel content of Kambalda glaukosphaerite suggests that glaukosphaerite at Kasompi is intimately intergrown, in a regular fashion, with nickeloan malachite.

Clearly, a further study of these materials by electron microprobe is essential to relate variations in chemistry to the phases present.

#### Kolwézite

Cobaltiferous malachite from Shaba (Zaire) was described by Deliens *et al.* (1973). Analyses show a cobalt content ranging from 0.25 to 18.46 wt. %. The X-ray powder patterns are generally similar to malachite for low cobalt content (0.25 to 4.22 wt. %) and to rosasite for the higher cobalt content (16.05 and 18.46 wt. %) (Jambor 1976b, p. 102). Recently the new name "kolwézite" was proposed by Deliens & Piret (1980) for the mineral represented by the latter two analyses with cobalt contents of 16.05 and 18.46%. These authors have deduced a triclinic cell for indexing the powder pattern of kolwézite. They also apply a similar triclinic indexing to the X-ray pattern of glaukosphaerite from Kasompi. If this interpretation of triclinic character is correct, there may be three phases in the Kasompi glaukosphaerite.

#### ACKNOWLEDGEMENTS

The authors acknowledge the assistance of several members of staff at CSIRO (Perth), the cooperation of M.W. Pryce of Government Chemical Laboratories (Perth) and of Dr. Sydney Hall of the University of Western Australia, and the kindness of Dr. Mincheva-Stefanova of the Mineralogical Museum, Sofia, who supplied a fragment of the original rosasite sample from Bakara, Bulgaria. The authors are also grateful for the valuable comments of the reviewers.

#### REFERENCES

- DELIENS, M. (1975): La glaukosphaerite de Kasompi (Shaba méridional, Zaire). *Soc. Franç. Minéral. Crist. Bull.* **98**, 175-178.
- , OOSTERBOSCH, R. & VERBEEK, T. (1973): Les malachites cobaltifères du Shaba méridional (Zaire). *Soc. Franç. Minéral. Crist. Bull.* **96**, 371-377.
- & PIRET, P. (1980): La kolwézite, un hydroxycarbonate de cuivre et de cobalt analogue à la glaukosphaerite et à la rosasite. *Bull. Mineral.* **103**, 179-184.

- ERD, R.C., GOFF, F.E., CESBRON, F.P. & CLARK, J.R. (1981): Mcguinnessite, a new carbonate from California. *Mineral. Record* **12**, 143-147.
- GÜNTER, J.R. & OSWALD, H.R. (1977): Crystal structure of  $Mg_2(OH)_2CO_3$ , deduced from the topotactic thermal decomposition of artinite. *J. Solid State Chem.* **21**, 211-215.
- JAMBOR, J.L. (1976a): A possible unit cell for glaukosphaerite. *Can. Mineral.* **14**, 574-576.
- (1976b): Studies of basic copper and zinc carbonates. 3. Powder X-ray data for zincian malachite, rosasite and cobalt analogues. *Geol. Surv. Can. Pap.* **76-1C**, 97-105.
- MANDARINO, J.A. (1976): The Gladstone-Dale relationship. I. Derivation of new constants. *Can. Mineral.* **14**, 498-502.
- MINCHEVA-STEFANOVA, I. (1961): Cuprozincite, rosasite and aurichalcite from the Vracha ore-district. *Inst. Geol. Bulgarian Acad. Sci. Bull.* **9**, 197-207.
- NICKEL, E.H. (1973): An occurrence of gaspéite and pecoraite in the Nullagine region of Western Australia. *Mineral Mag.* **39**, 113-115.
- , HALLBERG, J.A. & HALLIGAN, R. (1979): Unusual nickel mineralisation at Nullagine, Western Australia. *Geol. Soc. Aust. J.* **26**, 61-71.
- , ROBINSON, B.W., DAVIS, C.E.S. & MACDONALD, R.D. (1977): Otwayite, a new nickel mineral from Western Australia. *Amer. Mineral.* **62**, 999-1002.
- OSWALD, S.G. & CROOK, W.W., III (1979): Cuprohydromagnesite and cuproartinite, two new minerals from Gabbs, Nevada. *Amer. Mineral.* **64**, 886-889.
- PRYCE, M.W. & JUST, J. (1974): Glaukosphaerite, a new nickel analogue of rosasite. *Mineral. Mag.* **39**, 737-743.
- RAMSDELL, L.S. & WOLFE, C.W. (1950): The unit cell of malachite. *Amer. Mineral.* **35**, 119-121.
- STRUNZ, H. (1959): Tsumeb, seine Erze und Sekundärminerale, insbesondere der neu aufgeschlossenen zweiten Oxydationzone. *Fortsch. Mineral.* **37**, 87-90.
- SWANSON, H.E., COOK, M.I., EVANS, E.H. & de-GROOT, J.H. (1960): Standard X-ray diffraction powder patterns. 10. Data for 40 substances. *Nat. Bur. Standards Circ.* **539**.

Received September 1979, revised manuscript accepted January 1981.